Eur. Phys. J. Special Topics **156**, 175–182 (2008)

DOI: 10.1140/epjst/e2008-00614-2

THE EUROPEAN PHYSICAL JOURNAL SPECIAL TOPICS

Beyond the relativistic mean-field approximation: Configuration mixing of mean-field wave functions projected on angular momentum and particle number

T. Nikšić[a]

Physics Department, Faculty of Science, University of Zagreb, Croatia

Abstract. The framework of relativistic self-consistent mean-field models is extended to include correlations related to restoration of broken symmetries and to fluctuations of collective variables. The generator coordinate method is used to perform configuration mixing of angular-momentum and particle-number projected relativistic wave functions. The model, currently restricted to axially symmetric shapes, employs a relativistic point-coupling (contact) nucleon-nucleon effective interaction in the particle-hole channel, and a δ-interaction in the pairing channel. Both bulk and spectroscopic nuclear properties are explored.

1 Introduction

The rich variety of nuclear shapes far from stability has been the subject of extensive experimental and theoretical studies. Properties of heavy nuclei with a large number of active valence nucleons are best described in the framework of self-consistent mean-field models. A variety of structure phenomena, not only in medium-heavy and heavy stable nuclei, but also in regions of exotic nuclei far from the line of β-stability and close to the nucleon drip-lines, have been successfully described with mean-field models based on the Gogny interaction, the Skyrme energy functional, and the relativistic meson-exchange effective Lagrangian [1,2]. The self-consistent mean-field approach to nuclear structure represents an approximate implementation of Kohn-Sham density functional theory, which enables a description of the nuclear many-body problem in terms of a universal energy density functional. This framework, extended to take into account the most important correlations, provides a detailed microscopic description of structure phenomena associated with the shell evolution in exotic nuclei. When compared to the shell model, important advantages of the mean-field approach include the use of global effective nuclear interactions, the treatment of arbitrarily heavy systems including superheavy elements, and the intuitive picture of intrinsic shapes.

The erosion of spherical shell-closures in nuclei far from stability leads to deformed intrinsic states and, in some cases, mean-field potential energy surfaces with almost degenerate prolate and oblate minima. To describe nuclei with soft potential energy surfaces and/or small energy differences between coexisting minima, it is necessary to explicitly consider correlation effects beyond the mean-field level. The rotational energy correction, i.e. the energy gained by the restoration of rotational symmetry, is proportional to the quadrupole deformation of the intrinsic state and can reach several MeV for a well deformed configuration. Fluctuations of the quadrupole deformation also contribute to the correlation energy. Both types of correlations can be included simultaneously by mixing angular momentum projected states

[a] e-mail: tniksic@phy.hr

corresponding to different quadrupole moments. The most effective approach for configuration mixing calculations is the generator coordinate method (GCM), with multipole moments used as coordinates that generate the intrinsic wave functions.

2 The relativistic point-coupling model

In the model that we have developed in Refs. [3,4], the intrinsic wave functions are generated from constrained self-consistent solutions of the relativistic mean-field (RMF) equations for the point-coupling (PC) Lagrangian of Ref. [5]. For a complete discussion of the framework of relativistic point-coupling nuclear models we refer the reader to [5], and references therein. The specific choice of the PC Lagrangian defines the mean-field energy of a nuclear system

$$\begin{aligned} E_{RMF} &= \int d\boldsymbol{r}\ \mathcal{E}_{RMF}(\boldsymbol{r}) \\ &= \sum_k \int d\boldsymbol{r}\ v_k^2\ \bar{\psi}_k(\boldsymbol{r})\left(-i\boldsymbol{\gamma}\boldsymbol{\nabla}+m\right)\psi_k(\boldsymbol{r}) \\ &+ \int d\boldsymbol{r}\ \Big(\frac{\alpha_S}{2}\rho_S^2+\frac{\beta_S}{3}\rho_S^3+\frac{\gamma_S}{4}\rho_S^4+\frac{\delta_S}{2}\rho_S\triangle\rho_S+\frac{\alpha_V}{2}j_\mu j^\mu+\frac{\gamma_V}{4}(j_\mu j^\mu)^2+\frac{\delta_V}{2}j_\mu\triangle j^\mu \\ &+ \frac{\alpha_{TV}}{2}j_{TV}^\mu(j_{TV})_\mu+\frac{\delta_{TV}}{2}j_{TV}^\mu\triangle(j_{TV})_\mu+\frac{\alpha_{TS}}{2}\rho_{TS}^2+\frac{\delta_{TS}}{2}\rho_{TS}\triangle\rho_{TS}+\frac{e}{2}\rho_p A^0\Big), \end{aligned} \tag{1}$$

where ψ denotes the Dirac spinor field of a nucleon, and the local isoscalar and isovector densities and currents for a nucleus with A nucleons

$$\rho_S(\boldsymbol{r}) = \sum_k v_k^2\ \bar{\psi}_k(\boldsymbol{r})\psi_k(\boldsymbol{r}), \tag{2}$$

$$\rho_{TS}(\boldsymbol{r}) = \sum_k v_k^2\ \bar{\psi}_k(\boldsymbol{r})\tau_3\psi_k(\boldsymbol{r}), \tag{3}$$

$$j^\mu(\boldsymbol{r}) = \sum_k v_k^2\ \bar{\psi}_k(\boldsymbol{r})\gamma^\mu\psi_k(\boldsymbol{r}), \tag{4}$$

$$j_{TV}^\mu(\boldsymbol{r}) = \sum_k v_k^2\ \bar{\psi}_k(\boldsymbol{r})\gamma^\mu\tau_3\psi_k(\boldsymbol{r}), \tag{5}$$

are calculated in the *no-sea* approximation: the summation runs over all occupied states in the Fermi sea, i.e. only occupied single-nucleon states with positive energy explicitly contribute to the nucleon self-energies. v_k^2 denotes the occupation factors of single-nucleon states. In Eq. (1) ρ_p is the proton density, and A^0 denotes the Coulomb potential.

Here we only consider even-even nuclei that can be described by axially symmetric shapes. In addition to the axial symmetry, parity, symmetry with respect to the operator $e^{-i\pi\hat{J}_y}$, and time-reversal invariance are imposed as self-consistent symmetries. Time-reversal invariance implies that spatial components of the currents vanish in the nuclear ground state. The resulting single-nucleon Dirac equation reads

$$\left\{-i\boldsymbol{\alpha}\boldsymbol{\nabla}+V(\boldsymbol{r})+\beta\big(m+S(\boldsymbol{r})\big)\right\}\psi_i(\boldsymbol{r}) = \epsilon_i\psi_i(\boldsymbol{r}). \tag{6}$$

The eigensolutions are characterized by the projection of the total angular momentum along the symmetry axis (Ω_i), the parity (π_i), and the z-component of the isospin (t_i). The single-nucleon Dirac eigenvalue equation is solved by expanding the Dirac spinors in terms of eigenfunctions of an axially symmetric harmonic oscillator potential.

For an axially deformed nucleus the map of the energy surface as a function of the quadrupole moment is obtained by imposing a constraint on the mass quadrupole moment. The method of quadratic constraint uses an unrestricted variation of the function

$$\langle H\rangle\ +\ \frac{C}{2}\left(\langle\hat{Q}\rangle-\ q\right)^2, \tag{7}$$

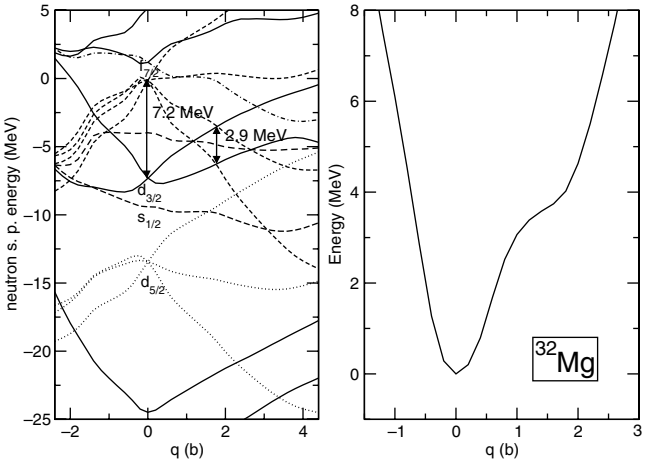

Fig. 1. The neutron single-particle levels for ^{32}Mg, as functions of the mass quadrupole moment. The thick dashed curve denotes the position of the Fermi energy (left panel). The binding energy curve for ^{32}Mg, calculated from the constrained solutions of the self-consistent relativistic mean-field equations.

where $\langle H \rangle$ is the total energy, $\langle \hat{Q} \rangle$ denotes the expectation value of the mass quadrupole operator, q is the deformation parameter, and C is the stiffness constant [8].

In addition to the self-consistent mean-field potential, for open-shell nuclei pairing correlations have to be included in the energy functional. In the current version, the model is not designed for nuclear systems very far from the valley of β-stability, and therefore a good approximation for the treatment of pairing correlations is provided by the BCS formalism. Following the prescription from Ref. [5], we use a δ-interaction in the pairing channel, supplemented with a smooth cut-off determined by the Fermi function of single-particle energies ϵ_k [6].

In the right panel of Fig. 1 we display the mean-field binding energy curve for ^{32}Mg as a function of the quadrupole moment, calculated with the PC-F1 [5] effective interaction. The constrained mean-field equation has been solved self-consistently on a regular mesh ranging from $q = -2.2\,\mathrm{b}$ to $q = 4.0\,\mathrm{b}$, with a mesh spacing of $\Delta q = 0.2\,\mathrm{b}$. In addition to the spherical ground state, the PC-F1 binding energy curve displays a prolate deformed shoulder at $q = 1.5\,\mathrm{b}$, at rather high excitation energy of $\approx 3.5\,\mathrm{MeV}$ above the ground state. The location of the shoulder can be related to the neutron single-particle levels calculated with the PC-F1 interaction, displayed in the left panel of Fig. 1. The ratio between the neutron spherical gap (7.2 Mev) and the gap at deformation $q = 1.5\,\mathrm{b}$ (2.9 MeV) is ≈ 2.5 for the PC-F1 interaction. Smaller ratio would lead to a more pronounced shoulder at lower excitation energy as shown in the calculations using the Gogny force [7].

3 Restoration of broken symmetries

3.1 Angular momentum projection

In the current version of the model the basis states $|\phi(q)\rangle$ are Slater determinants of single-nucleon states generated by solving the constrained RMF + BCS equations, as described in the previous section. Since the axially deformed mean field breaks rotational symmetry, the basis states $|\phi(q)\rangle$ are not eigenstates of the total angular momentum. To be able to compare theoretical predictions with empirical data, it is necessary to construct states with good angular momentum. The projected wave functions are obtained by employing the standard projection technique described in Ref. [8]

$$\left|\phi^{JM}(q)\right\rangle = \sum_K \hat{P}^J_{MK} \left|\phi(q)\right\rangle, \tag{8}$$

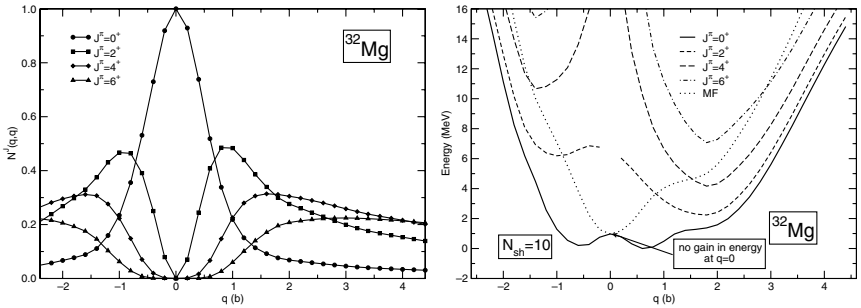

Fig. 2. Projected norm overlap kernel $\mathcal{N}^J(q,q)$ (left panel) and angular momentum projected potential energy curves (right panel) as functions of the mass quadrupole moment for ^{32}Mg.

where $\hat{P}^J_{MK}$ denotes the angular momentum projection operator

$$\hat{P}^J_{MK} = \frac{2J+1}{8\pi^2} \int d\Omega D^{J*}_{MK}(\Omega) \hat{R}(\Omega). \tag{9}$$

The integration is performed over the three Euler angles α, β, and γ. The operator $D^J_{MK}(\Omega) = e^{-iM\alpha} d^J_{MK}(\beta) e^{-iK\gamma}$ is the Wigner function, and $\hat{R}(\Omega) = e^{-i\alpha\hat{J}_z} e^{-i\beta\hat{J}_y} e^{-i\gamma\hat{J}_z}$ is the rotation operator. The restriction to axially symmetric ($\hat{J}_z \left|\phi(q)\right\rangle = 0$) configurations simplifies the problem considerably, because in this case the integrals over the Euler angles α and γ can be performed analytically. For an arbitrary multipole operator $\hat{Q}_{\lambda\mu}$ we thus find

$$\left\langle\phi(q)\right| \hat{Q}_{\lambda\mu} \hat{P}^J_{MK} \left|\phi(q)\right\rangle = \frac{2J+1}{2} \delta_{M-\mu}\delta_{K0} \int_0^\pi \sin\beta d^{J*}_{-\mu 0}(\beta) \left\langle\phi(q)\right| \hat{Q}_{\lambda\mu} e^{-i\beta\hat{J}_y} \left|\phi(q)\right\rangle d\beta. \tag{10}$$

We notice that this expression vanishes for odd values of angular momentum J, i.e., the projected quantities are defined only for even values of J. The kernels $\left\langle\phi(q)\right| \hat{Q}_{\lambda\mu} e^{-i\beta\hat{J}_y} \left|\phi(q)\right\rangle$ can be evaluated by employing the generalized Wick theorem.

In the left panel of Fig. 2 we display the projected norms $\mathcal{N}^J(q) = \left\langle \phi^J(q)\right| \left.\phi^J(q)\right\rangle$ that give the probability for angular momentum J in various intrinsic wave functions $\left|\phi(q)\right\rangle$. The spherical configuration is a pure 0^+ state, hence $\mathcal{N}^{J=0}(0) = 1$ and $\mathcal{N}^{J=2,4,\cdots}(0) = 0$. The maxima of the projected norm overlap kernels for higher angular momenta are correspondingly shifted to larger deformations.

For each intrinsic configuration $\left|\phi(q)\right\rangle$ we calculate the projected energy

$$E^J(q) = \frac{\mathcal{H}^J(q,q)}{\mathcal{N}^J(q,q)} = \frac{\left\langle\phi(q)\right| \hat{H} P^J_{00} \left|\phi(q)\right\rangle}{\left\langle\phi(q)\right| P^J_{00} \left|\phi(q)\right\rangle}. \tag{11}$$

The results are displayed in the right panel of Fig. 2, together with the mean-field binding energy curve. Since the spherical configuration is already a pure 0^+ state, there is no energy gain for $J^\pi = 0^+$ at $q = 0$ b. Notice that the spherical point is not included in plots of $E^J(q)$ for $J \geq 2$. Namely, for $J \neq 0$ the quantities $\mathcal{H}^J(0,0)$ and $\mathcal{N}^J(0,0)$ are so small that their ratio Eq. (11) cannot be determined accurately. For higher values of the angular momentum ($J^\pi = 6^+, 8^+$ in Fig. 2) several additional configurations close to the spherical point are also characterized by very small values of the projected norm overlap kernel. These configurations can be safely omitted from the projected energy curves, because on the one hand the angular momentum projection becomes inaccurate at these points, and on the other hand the corresponding angular momentum projected states would not play any role in configuration mixing calculations.

The $J = 0$ projected energy curve displays two almost degenerate minima at small oblate and prolate deformations. This feature is common to all nuclei for which the mean-field calculation predicts a spherical ground state [7]. As compared to the mean-field energy, the prolate deformed

shoulder is more pronounced, and its excitation energy has been lowered from 3.5 to 1.2 MeV by angular momentum projection. However, in the present calculation with the PC-F1 interaction, the gain in rotational energy is too small to deform the ground state of ^{32}Mg. This result is in contrast with the available experimental data and with calculations based on the Gogny interaction [7]. The different predictions for the ground state of ^{32}Mg can be related to the corresponding mean-field binding energy curves and, more specifically, to the different results for the size of the $N = 20$ neutron gap, obtained with the Gogny and PC-F1 effective interaction.

3.2 Particle number projection

The principal disadvantage of describing pairing correlations in the BCS approximation is that the resulting wave function is not an eigenstate of the particle number operator. More precisely, the BCS ground state contains admixtures of particle-number eigenstates with a relative spread of order $1/\sqrt{N}$, where N denotes the average number of valence particles. The ideal solution, of course, is to perform particle number projection from the BCS state before variation. This procedure is technically rather complicated and very much time consuming, and therefore it is usual to employ the Lipkin-Nogami (LN) approximation to the exact particle number projection. States with good angular momentum and particle number are then obtained by performing projections from the mean-field plus LNBCS solution

$$\left|\phi^{JM}(q)\right\rangle = \sum_K \hat{P}^J_{MK} \hat{P}^Z \hat{P}^N \left|\phi(q)\right\rangle. \tag{12}$$

The particle-number projection operators read

$$\hat{P}^N = \frac{1}{2\pi} \int_0^{2\pi} d\phi_n e^{i(\hat{N}-N)\phi_n} \ , \qquad \hat{P}^Z = \frac{1}{2\pi} \int_0^{2\pi} d\phi_p e^{i(\hat{N}-Z)\phi_p} \ . \tag{13}$$

where $\hat{N}$ is the number operator, and $N(Z)$ denotes the number of neutrons (protons).

4 Configuration mixing

Fluctuations of quadrupole deformation represent an additional source of correlation energy. Both types of correlations can be included simultaneously by mixing angular-momentum and particle-number projected states corresponding to different quadrupole moments. The configuration mixing is performed with the generator coordinate method. A detailed review of the GCM can be found in Chapter 10 of Ref. [8]. The method is based on the assumption that, starting from a set of basis states $|\phi(q)\rangle$ that depend on a collective coordinate q, one can build approximate eigenstates of the nuclear Hamiltonian. The basis states used in the present version of the model are the axially deformed mean-field plus LNBCS solutions. They break rotational symmetry, while the particle number is only approximately restored with the Lipkin-Nogami procedure. Therefore, the correlated wave function is constructed as a linear combination of the angular-momentum and particle-number projected basis states

$$\left|\Psi^{JM}_\alpha\right\rangle = \sum_{j,K} f^{JK}_\alpha(q_j) \hat{P}^J_{MK} \hat{P}^Z \hat{P}^N \left|\phi(q_j)\right\rangle. \tag{14}$$

The weight functions $f^J_\alpha(q)$, together with the corresponding energies of the correlated states E^J_α, are determined by solving the Hill-Wheeler (HW) equation [8]

$$\sum_j \mathcal{H}^J(q_i, q_j) f^J_\alpha(q_j) = E^J_\alpha \sum_j \mathcal{N}^J(q_i, q_j) f^J_\alpha(q_j), \tag{15}$$

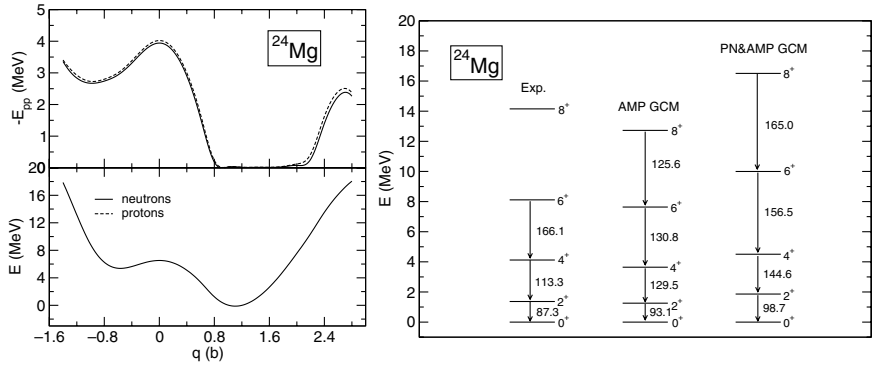

Fig. 3. The BCS pairing energy for protons and neutron (upper left panel), and the mean-field plus BCS binding energy curve (lower left panel) of ^{24}Mg, as functions of the mass quadrupole moment. The GCM spectra calculated with (PN&AMP), and without (AMP) particle number projection in comparison to the experimental ground-state band [11] (right panel).

which contains the projected norm $\mathcal{N}^J(q_i, q_j) = \langle q_i | \hat{P}^J_{00} \hat{P}^N \hat{P}^Z | \phi(q_j) \rangle$ and the projected Hamiltonian kernel $\mathcal{H}^J(q_i, q_j) = \langle q_i | \hat{H} \hat{P}^J_{00} \hat{P}^N \hat{P}^Z | \phi(q_j) \rangle$. The Hill-Wheeler equation represents a generalized eigenvalue problem. Thus the weight functions $f^J_\alpha(q_i)$ are not orthogonal and cannot be interpreted as collective wave functions for the variable q. The standard procedure is to re-express Eq. (15) in terms of another set of functions, $g^J_\alpha(q_i)$, defined by

$$g^J_\alpha(q_i) = \sum_j (\mathcal{N}^J)^{1/2}(q_i, q_j) f^J_\alpha(q_j). \tag{16}$$

The functions $g^J_\alpha(q_i)$ are orthonormal and play the role of collective wave functions. For completeness we also include the expressions for physical observables, such as transition probabilities and spectroscopic quadrupole moments [7]. The reduced transition probability for a transition between an initial state (J_i, α_i), and a final state (J_f, α_f), reads

$$B(E2; J_i\alpha_i \to J_f\alpha_f) = \frac{e^2}{2J_i + 1} \left| \sum_{q_f, q_i} f^{J_f *}_{\alpha_f}(q_f) \langle J_f q_f | \, | \hat{Q}_2 | \, | J_i q_i \rangle f^{J_i}_{\alpha_i}(q_i) \right|^2, \tag{17}$$

and the spectroscopic quadrupole moment for a state $(J\alpha)$ is defined

$$Q^{spec}(J, \alpha) = e \sqrt{\frac{16\pi}{5}} \begin{pmatrix} J & 2 & J \\ J & 0 & -J \end{pmatrix} \sum_{q_i, q_j} f^{J*}_\alpha(q_i) \langle J q_i | \, | \hat{Q}_2 | \, | J q_j \rangle f^J_\alpha(q_j). \tag{18}$$

Since these quantities are calculated in full configuration space, there is no need to introduce effective charges, hence e denotes the bare value of the proton charge.

In Fig. 3 we display the pairing energy (upper left panel), and the total RMF binding energy curve (lower left panel) of ^{24}Mg, as functions of the mass quadrupole moment. The Lipkin-Nogami procedure has not been implemented at this stage, and consequently pairing correlations vanish in a broad region of deformations around the deformed first minimum of the potential energy surface. Since the moment of inertia of a rotational band is reduced in the presence of pairing correlations, dynamical pairing effects could be important in the description of the ground-state band of ^{24}Mg.

The GCM excitation energies and the resulting transition probabilities for the ground-state band, calculated with the PC-F1 effective interaction, are shown in the right panel of Fig. 3. The results of the AMP and PN&AMP configuration mixing calculations are compared with the data. In the following AMP will indicate that only angular momentum projection has been carried out before GCM configuration mixing (i.e., the model of Ref. [3] is used), and PN&AMP

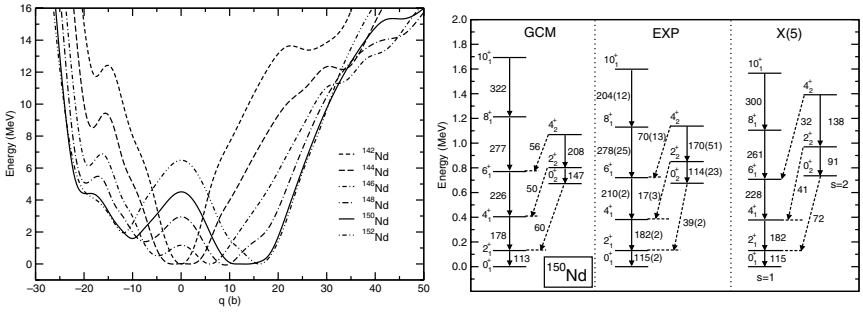

Fig. 4. Self-consistent RMF binding energy curves of $^{142-152}$Nd, as functions of the mass quadrupole moment (right panel). The particle-number projected GCM spectrum of ^{150}Nd, compared with the experimental data [15] and the X(5)-symmetry predictions for the excitation energies, intraband and interband B(E2) values (in Weisskopf units) of the ground state (s = 1) and β_1 (s = 2) bands (right panel).

will denote the results of the GCM calculations which include both the restoration of the particle number and rotational symmetry. As expected, the inclusion of dynamical pairing effects reduces the moment of inertia, but the resulting spectrum is too much spread out compared to experiment. This is a well known problem, related to the fact that we project particle number and angular momentum only after variation, rather than performing the projections before variation. It has been shown that in the latter case rotational bands with larger moments of inertia are obtained, provided that the model geometry allows for the alignment of nucleon angular momenta. Since the full projection before variation is technically and computationally much more complex, it has been seldom used in realistic calculations. The transition probabilities, as well as the calculated spectroscopic quadrupole moment $Q_{spec}(2_1^+) = -16.56\,\mathrm{e\,fm}^2$, are in very good agreement with the data.

5 Microscopic description of quantum shape phase transitions

We have applied the relativistic GCM to the study of nuclear quantum phase transitions (QPT) [10]. In the case of atomic nuclei first- and second-order QPT can occur between systems characterized by different ground-state shapes. Nuclear shape phase transitions have been the subject of numerous theoretical and experimental studies. For recent reviews we refer the reader to [12,13].

In the left panel of Fig. 4 we plot the self-consistent RMF+LN BCS potential energy curves (PEC) of $^{142-152}$Nd, as functions of the mass quadrupole moment. The PECs display a gradual transition between spherical ^{142}Nd and strongly prolate deformed ^{152}Nd. Of particular interest is the PEC of ^{150}Nd which exhibits a wide flat minimum on the prolate side ($\gamma = 0°$), with an additional minimum at $\approx 1.8\,\mathrm{MeV}$ excitation energy and an oblate ($\gamma = 60°$) deformation. The two minima are separated by a potential barrier of $\approx 4.5\,\mathrm{MeV}$. One notes the similarity between the PEC of ^{150}Nd and the projections on the $\gamma = 0°$ (prolate) and $\gamma = 60°$ (oblate) axes of the original X(5) potential considered by Iachello in Ref. [14] (square well in the variable β, and harmonic oscillator potential in γ). Although particular isotopes exhibit relatively flat PECs over an extended range of the deformation parameter, characteristic for critical point symmetries, simple mean-field approach cannot be used for a quantitative analysis of critical point symmetries. The concept of shape phase transition includes analytic expressions for observables: excitation eneregies and B(E2) rates, and this is not possible on the mean-field level.

Correlation effects related to the restoration of broken symmetries and to fluctuations of collective coordinates are taken into account by performing configuration mixing calculations of projected states. For ^{150}Nd we have thus solved the GCM equations in the basis of constrained mean-field + LN BCS Slater determinants, projected on angular momentum and particle number. The GCM results for the two lowest bands are compared in the right panel of Fig. 4 with

the available data [15], and with the X(5)-symmetry predictions for the excitation energies, intraband B(E2) values (in Weisskopf units) of the ground state ($s = 1$) and β_1 ($s = 2$) bands, and interband transitions between the ($s = 2$) and ($s = 1$) bands. To facilitate the comparison with the X(5) spectrum, which corresponds to the solution around $\gamma = 0°$ [14], the GCM results in Fig. 4 have been obtained by performing configuration mixing calculations only on the prolate side. In fact, since the basis of deformed states does not include the full range of γ-values ($0° \leq \gamma \leq 60°$), configuration mixing must be performed only on the prolate side in order to remain close to the phase-transitional region in which X(5) occurs. The theoretical spectra are normalized to the experimental energy of the 2_1^+ state. We note the excellent agreement of the GCM spectrum both with the data and with the X(5)-symmetry predictions.

6 Summary and outlook

The very successful relativistic mean-field framework has been extended to explicitly include correlations related to the restoration of broken symmetries and to fluctuations of collective coordinates. There are, of course, many possible improvements and extensions of the present implementation of the relativistic GCM model. Perhaps the most obvious is the extension to shapes that are not constrained by axial symmetry. The inclusion of triaxial deformations is in principle straightforward but, because it requires an enormous increase of computational capabilities, not feasible at present. The second major problem is that the present GCM configuration mixing calculations correspond to a projection after variation. A more general variation after projection is far too complicated to be used in realistic calculations at the present stage. A possible improvement, however, is to generate the GCM basis functions, for each value of the angular momentum, by performing cranking RMF+LNBCS calculations with the additional constraint $\langle J_x \rangle = J$. This would automatically increase the moments of inertia of rotational bands, and therefore produce spectra in better agreement with experiment. Finally, let us emphasize again one of the conclusions of Ref. [3], namely that those correlations which are explicitly treated in the GCM configuration mixing, should not be contained in the effective interaction in an implicit way, i.e. by adjusting the parameters of the interaction to data which already include these correlations. Therefore, new global effective interactions are needed, which will not contain rotational energy corrections and quadrupole fluctuation correlations.

References

1. M. Bender, P.-H. Heenen, P.-G. Reinhard, Rev. Mod. Phys. **75**, 121 (2003)
2. D. Vretenar, A.V. Afanasjev, G.A. Lalazissis, P. Ring, Phys. Rep. **409**, 101 (2005)
3. T. Nikšić, D. Vretenar, P. Ring, Phys. Rev. C **73**, 034308 (2006)
4. T. Nikšić, D. Vretenar, P. Ring, Phys. Rev. C **74**, 064309 (2006)
5. T. Bürvenich, D.G. Madland, J.A. Maruhn, P.-G. Reinhard, Phys. Rev. C **65**, 044308 (2002)
6. S.J. Krieger, P. Bonche, H. Flocard, P. Quentin, M.S. Weiss, Nucl. Phys. A **517**, 275 (1990)
7. J.L. Egido, L.M. Robledo, in *Extended Density Functionals in Nuclear Structure Physics*, Lecture Notes in Physics, edited by G.A. Lalazissis, P. Ring, D. Vretenar (Springer-Verlag, Heidelberg, 2004), Vol. 641
8. P. Ring, P. Schuck, *The Nuclear Many-Body Problem* (Springer-Verlag, New York, 1980)
9. A. Valor, P.-H. Heenen, P. Bonche, Nucl. Phys. A **671**, 145 (2000)
10. T. Nikšić, D. Vretenar, G.A. Lalazissis, P. Ring, Phys. Rev. Lett. **99**, 092502 (2007)
11. P.M. Endt, Nucl. Phys. A **510**, 1 (1990)
12. J. Jolie, R.F. Casten, Nucl. Phys. News **15**, 20 (2005)
13. R.F. Casten, Nat. Phys. **2**, 811 (2006)
14. F. Iachello, Phys. Rev. Lett. **85**, 3580 (2000); **87**, 052502 (2001)
15. R. Krücken et al., Phys. Rev. Lett. **88**, 232501 (2002)